Journal of Magnetic Resonance 213 (2011) 98–106

Contents lists available at SciVerse ScienceDirect

Journal of Magnetic Resonance

journal homepage: www.elsevier.com/locate/jmr

^{14}N quadrupole resonance and ^{1}H T_1 dispersion in the explosive RDX ☆

John A.S. Smith [a], Martin Blanz [b], Timothy J. Rayner [c], Michael D. Rowe [a,*], Simon Bedford [d], Kaspar Althoefer [a]

[a] Department of Informatics, King's College London, Strand, London WC2R 2LS, UK
[b] Doerrigsgarten 7, D-Celle 29221, Germany
[c] Tronning, Grange Road, Crawley Down, West Sussex RH10 4JT, UK
[d] 14064 Old Station Rd., Poway, CA 92064, USA

ARTICLE INFO

Article history:
Received 25 June 2011
Revised 31 August 2011
Available online 10 September 2011

Keywords:
RDX
Magnetic field cycling NMR
T_1 dispersion
Quadrupole dips
^{14}N NQR

ABSTRACT

The explosive hexahydro-1,3,5-trinitro-s-triazine $(CH_2–N–NO_2)_3$, commonly known as RDX, has been studied by ^{14}N NQR and ^{1}H NMR. NQR frequencies and relaxation times for the three ν_+ and ν_- lines of the ring ^{14}N nuclei have been measured over the temperature range 230–330 K. The ^{1}H NMR T_1 dispersion has been measured for magnetic fields corresponding to the ^{1}H NMR frequency range of 0–5.4 MHz. The results have been interpreted as due to hindered rotation of the NO_2 group about the N–NO_2 bond with an activation energy close to 92 kJ mol^{-1}. Three dips in the ^{1}H NMR dispersion near 120, 390 and 510 kHz are assigned to the ν_0, ν_- and ν_+ transitions of the $^{14}NO_2$ group. The temperature dependence of the inverse line-width parameters T_2^* of the three ν_+ and ν_- ring nitrogen transitions between 230 and 320 K can be explained by a distribution in the torsional oscillational amplitudes of the NO_2 group about the N–NO_2 bond at crystal defects whose values are consistent with the latter being mainly edge dislocations or impurities in the samples studied. Above 310 K, the ^{14}N line widths are dominated by the rapid decrease in the spin–spin relaxation time T_2 due to hindered rotation of the NO_2 group. A consequence of this is that above this temperature, the ^{1}H T_1 values at the quadrupole dips are dominated by the spin mixing time between the ^{1}H Zeeman levels and the combined ^{1}H and ^{14}N spin–spin levels.

1. Introduction

The explosive RDX (hexahydro-1,3,5-trinitro-s-triazine or cyclo-trimethylene-trinitramine) has three polymorphs, α and β at ambient conditions and γ at high pressure [1]. β-RDX is so unstable that its crystal structure is unknown and under normal conditions RDX exists only as the α polymorph which neutron diffraction crystal analysis [2] has shown to have the structural conformation shown in Fig. 1. The hexahydro-s-triazine ring is in the chair conformation with two nitro groups positioned differently from the third and in the crystal lattice pairs of RDX molecules interact [3] so that all three ring nitrogens and nitro groups are crystallographically unique and give rise to separate groups of NQR lines. There are many publications dealing with fundamental aspects of RDX ^{14}N NQR and also its application in the field of explosive detection (see for example [3–8]). The ^{1}H NMR line-shape and spin–lattice relaxation time T_1 of RDX at the fixed frequency of 56.4 MHz [9] has also been analysed and related to proton–proton distances. Further information about molecular geometry and interactions in crystalline RDX has come from the theoretical analysis of terahertz spectra [10–12] and vibrational photoacoustic spectra [13]. In this paper we present measurements of the ^{1}H NMR T_1 dispersion for RDX in the frequency ranges 1.7–1000 kHz, 3300–3535 kHz and 5000–5400 kHz and compare them with NQR results in order to show that much of the NQR behaviour can be understood in terms of hindered rotation of the NO_2 groups in this molecule about the N–NO_2 bond with an activation energy close to 92 kJ mol^{-1} as well as the torsional oscillations about the same bond.

2. Experimental methods

The ^{1}H T_1 dispersion measurements were conducted on a fast field cycling NMR spectrometer as described previously [14] and the ^{14}N NQR studies on S.M.I.S and Tecmag "Libra" pulsed RF spectrometers. The sample for the NMR work was RDX stabilised in Galden oil and for the NQR study was PE4 (approximately 88% RDX). The measurements are mainly confined to temperatures which might apply in the application of NQR to explosive

☆ This work was funded in part by the UK Defence Science and Technology Laboratory (DSTL Fort Halstead).
* Corresponding author. Fax: +44 20 7848 2699.
E-mail addresses: john.smith@kcl.ac.uk (J.A.S. Smith), Familie.Blanz@kabelmail.de (M. Blanz), tjrayner@tiscali.co.uk (T.J. Rayner), michael.d.rowe@kcl.ac.uk (M.D. Rowe), simonbedford@cox.net (S. Bedford), k.althoefer@kcl.ac.uk (K. Althoefer).

1090-7807/$ - see front matter © 2011 Elsevier Inc. All rights reserved.
doi:10.1016/j.jmr.2011.09.011

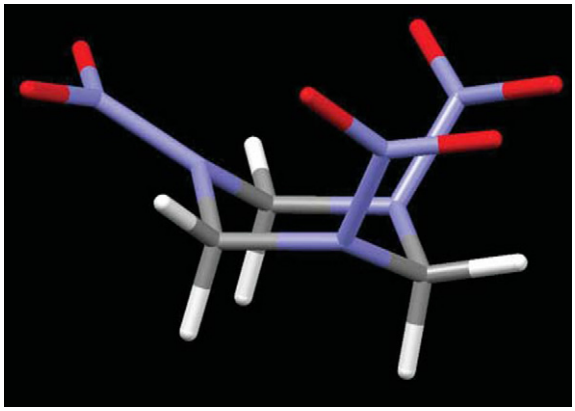

Fig. 1. The molecular structure of α-RDX reproduced from [1] by kind permission of Prof. Colin R. Pulham. The carbon, hydrogen, oxygen and nitrogen atoms are coloured grey, white, red and blue respectively. (For interpretation of the references to colour in this figure legend, the reader is referred to the web version of this article.)

detection. Because of the very fast switching rate in the NMR field cycling studies, (approximately 6×10^{10} Hz s^{-1}), level crossing effects are neglected.

3. Results and discussion

3.1. ^1H T_1 dispersion measurements

We have carried out ^1H NMR T_1 dispersion measurements for RDX at various temperatures in the frequency region between 1.7 kHz and 1 MHz in which the NQR transitions from the NO_2 groups occur and also in the two regions, centred on 5.2 and 3.4 MHz, where the ν_+ and ν_- NQR transitions of the ring ^{14}N nuclei lie. It is these latter higher frequency transitions that have been used in the NQR detection of RDX, particularly in airline luggage [15,16]. Our ^1H T_1 dispersion measurements for the low frequency range at four different temperatures are shown in Fig. 2. The variation of ^1H T_1 at 322 K bears some resemblance to the ^1H T_1 dispersion in PETN over the same frequency range (Fig. 6 of Ref. [14]). Both have an initial region, up to about 80 kHz here for RDX, where T_1 rises sharply followed by a second region with quadrupole dips.

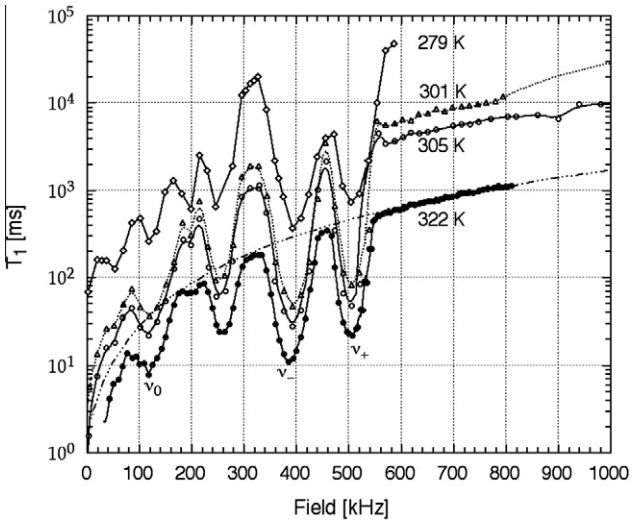

Fig. 2. The ^1H NMR T_1 dispersion in RDX below 1 MHz at four different temperatures.

By analogy to our interpretation for PETN [14] we attribute the relaxation mechanism in the initial region for RDX to a transient twist of the CH_2 groups caused by hindered rotation of the neighbouring NO_2 groups about the N–N bond. Since the NO_2 groups do not sit on symmetry axes, the N–O distances and ONO angles in all three nitro groups differ and each rotation is likely to involve a significant transient change in their environment. The second region here for RDX shows four quadrupole dips with frequencies close to 120, 260, 390 and 510 kHz at 322 K and these can be attributed to cross-relaxation with the ^{14}N nuclei of the NO_2 groups at frequencies which are known from zero-field pulsed NQR measurements. The ^{14}N ν_+ lines of the NO_2 groups of RDX at room temperature have been observed [17] at 502.3, 500.5 kHz and the ν_- lines at 405.1, 396.2 and 384.1 kHz. So the quadrupole dips observed here at 510, 390 and 120 kHz can be assigned to the ν_+, ν_- and ν_0 ^{14}N NQR frequencies respectively. The dip near 260 kHz is probably due to two-frequency cross-relaxation of the ν_+ transitions near 510 kHz. Other weak dips are observed at low frequency in the 279 K data: the dip near 60 kHz is assigned to a two-proton jump for ν_0 at 120 kHz, that near 200 kHz the same for the ν_- transition at 385 kHz and that close to 240 kHz the same for the ν_+ transition near 510 kHz.

The low-field ^1H T_1 dispersion results for RDX have been analysed in the same way as for PETN [14]. Plots of $1/T_1$ versus proton NMR frequency up to 80 kHz for the 301 and 305 K low field T_1 data of Fig. 2 were fitted using Eqs. (1)–(3); assuming equal probability for the occupation of the two sites involved in the reorientation.

$$\left[\frac{1}{T_1}\right] = C\left(\frac{\tau_c}{1+(\omega_H+\omega_L)\tau_c)^2} + \frac{4\tau_c}{1+4(\omega_H+\omega_L)\tau_c)^2}\right) \quad (1)$$

with

$$C = \frac{3}{80}\gamma_H^4\hbar^2\left(\frac{\mu_0}{4\pi}\right)^2\frac{\sin^2(2\alpha_{HH})}{r_{HH}^6} \quad (2)$$

and

$$\tau_c = \tau_0 e^{(E_a/RT)} \quad (3)$$

where $2\alpha_{HH}$ is the small transient change in the angular orientation of the interproton vector of the CH_2 group of length r_{HH}, γ_H is the proton gyromagnetic ratio and $\omega_H = 2\pi\nu_H$ and $\omega_L = 2\pi\nu_L$, where ν_H and ν_L are the ^1H NMR frequencies in the applied magnetic field and in the local dipolar field (assumed to be 32 kHz [9]) respectively. τ_c is the correlation time and E_a the activation energy characterising the motion. The fits gave approximate values for τ_c of 3 ms and E_a of 40 kJ mol^{-1}. However, the value for C is unacceptably large, which is probably explained by overlap with the ν_0 transition near 120 kHz, which would be expected to have sub-harmonics near 60 and 40 kHz due respectively to two or three relaxation jumps, one of which may actually be observed close to 60 kHz in the dispersion data at 279 K. These transitions may even overlap the dipolar absorption edge and so be partly responsible for the short ^1H T_1 in low or zero field. We have less data points in this low frequency region for RDX compared to in our previous study of PETN [14] and the values of τ_c and E_a are therefore very tentative, particularly as the expected low-field plateau has not been reached.

In the high frequency limit when $[(\omega_H+\omega_L)^2\tau_c^2] \gg 1$ we can write Eq. (1) as

$$T_1 = \frac{\tau_c}{2C}(\omega_H+\omega_L)^2 = \frac{2\pi^2\tau_c}{C}(\nu_H+\nu_L)^2 \quad (4)$$

A fit with Eq. (4) to the "off-dip" or background T_1 values for the 322 K data is also shown in Fig. 2 and as can be seen, from about 180 kHz upwards this high frequency limit is closely followed, as would be expected with the long τ_c of 3 ms.

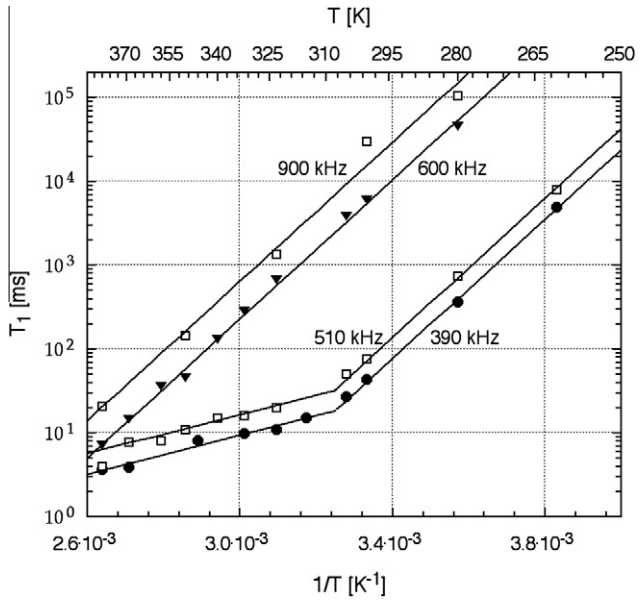

Fig. 3. Arrhenius plot of the temperature dependence of the ^{1}H NMR T_1 of RDX measured by field cycling at on-dip frequencies of 390 and 510 kHz and off-dip frequencies of 600 and 900 kHz.

Since in Eq. (3) τ_c is defined by an Arrhenius equation, then in the high frequency limit, the temperature dependence of T_1 at a fixed frequency has the same form. This can be seen by substituting τ_c from Eq. (3) into Eq. (4) and rearranging to give

$$T_1 = \frac{2\pi^2\tau_0(\nu_H+\nu_L)^2}{C}e^{(E_a/RT)} = Ae^{(E_a/RT)} \quad (5)$$

or

$$\ln(T_1) = \ln(A) + \frac{E_a}{R}\left(\frac{1}{T}\right) \quad (6)$$

We have measured the ^{1}H NMR T_1 of RDX by field cycling at temperatures between 260 and 380 K at four fixed frequencies, two "on-dip" at 390 and 510 kHz and two "off-dip" at 600 and 900 kHz. The results are presented in the Arrhenius plot of Fig. 3. The plots of the "off-dip" T_1 values at 600 and 900 kHz are indeed simple linear plots and fits are shown using Eq. (6), from the slope of which we obtain a value for E_a of 80 kJ mol^{-1}. As might be expected the plots of the "on-dip" T_1 values at 390 and 510 kHz show different behaviour, there are two linear regions with a marked change in slope around 310 K and Fig. 3 shows fits to each region again using Eq. (6). Below 310 K the slope of the linear fit is the same as for the "off-dip" plots so again E_a is 80 kJ mol^{-1} but above 310 K we obtain a value for E_a of 22 kJ mol^{-1}. It is likely that because of the dipolar splitting of the ^{1}H Zeeman levels, avoided level crossing [18] will be the predominant mechanism. At "on-dip" frequencies, spin–lattice relaxation is expected to occur in two stages: in the first, the spin temperatures of the Zeeman and spin–spin systems equalise, usually in a short time, and in the second, the common spin temperature then relaxes towards its equilibrium value. The results in Fig. 3 suggest that in fact above 310 K the first step becomes rate determining between 310 and 385 K. In logarithmic plots, the temperature coefficients are -2.65×10^{-3} K^{-1} 390 kHz and -2.78×10^{-3} K^{-1} at 510 kHz, identical within experimental error. However, because of the comparable values of the two times in this region, the conditions are non-adiabatic and a single exponential time constant is unlikely to be valid. In this rather restricted temperature range, T_1 can be equally well fitted to a linear variation with temperature with coefficients of

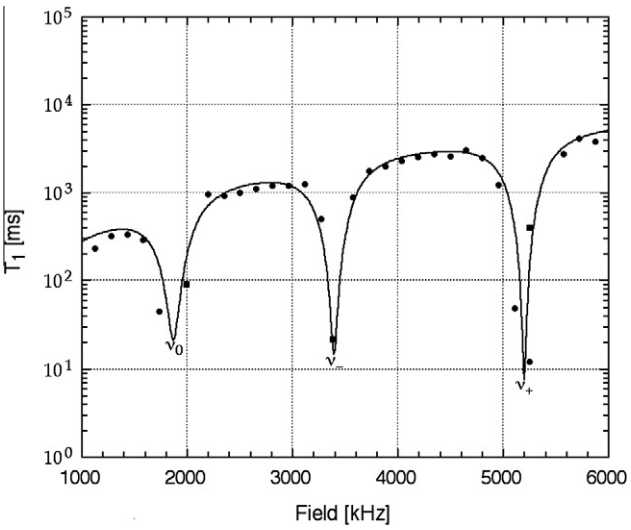

Fig. 4. A low resolution ^{1}H NMR T_1 dispersion measurement for RDX at 355 K showing the location of the three ring nitrogen quadrupole dips.

-0.17 ms K^{-1} at 390 kHz and -0.28 ms K^{-1} at 510 kHz; a mean value of -0.23 ms K^{-1}. It should be noted that in the solid phase, the average internuclear distance between a given ring N atom and any of the four nearest CH_2 protons is 209 pm [2], corresponding to a mean dipolar coupling constant of $\gamma_N\gamma_H\hbar/r_{NH}^3(\mu_0/4\pi) = 6.0$ kHz, which would lead one to expect a faster spin mixing time between the two spin systems rather than the values observed in RDX, e.g. 10 ms at 305 K. Part of the reason is a consequence of the quenching of the dipolar ^{14}N···^{1}H coupling in first order when the asymmetry parameter is non-zero, which in RDX would reduce the dipolar coupling constant by a factor of six [19]. Another factor may be that because of the non-adiabatic conditions there is slower spin mixing between the states $|x,-\rangle$ and $|z,+\rangle$ than expected (here x, z and +, − denote the ^{14}N quadrupole states and the ^{1}H magnetic states respectively). Slow spin mixing has also been observed in other compounds containing nitro groups in which spin-mixing times as long as 100 ms have been observed [18,20].

The ^{14}N NQR transitions from the RDX ring nitrogen atoms lie in the frequency range 1000–6000 kHz and Fig. 4 shows a plot of data

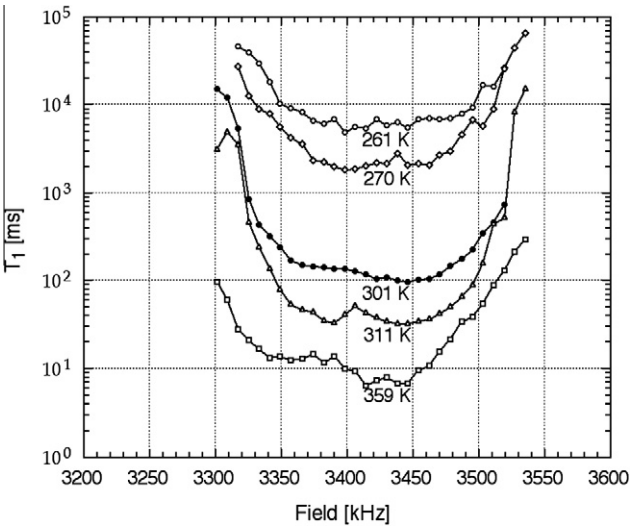

Fig. 5. ^{1}H NMR T_1 dispersion measurements for RDX in the region of the ring nitrogen ν_- quadrupole dip (for clarity only the results for five temperatures are shown).

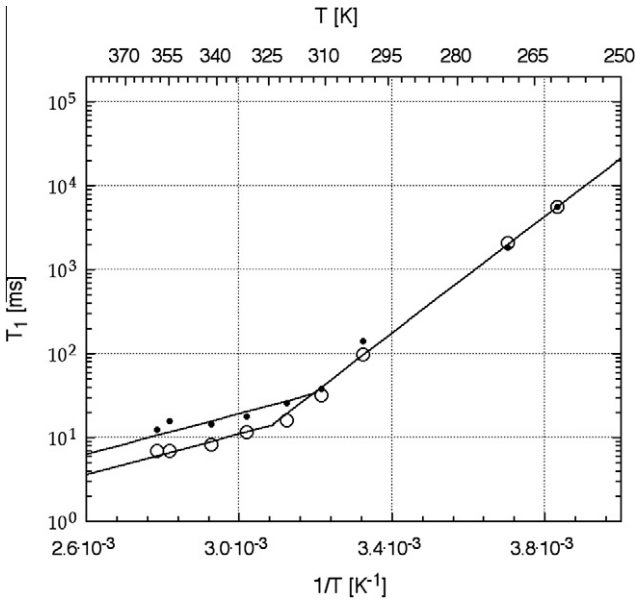

Fig. 6. Arrhenius plot of the temperature dependence of the ^{1}H NMR T_1 at the minima of the low (●) and high (○) frequency features of the ring nitrogen ν_- dip in Fig. 5, for the full range of temperatures studied.

from a low resolution ^{1}H NMR T_1 dispersion measurement over this range for RDX at 355 K together with a fit using Lorentzian functions for each of the three dips and a power law for the background. Clearly this plot has too few data points to give an accurate representation of the quadrupole dips but it provides an overview of the full high frequency range. We have carried out detailed measurements in the vicinity of the ring nitrogen ν_- and ν_+ quadrupole dips. Variable temperature ^{1}H T_1 dispersion measurements were carried out over the ν_- dip region in the range of 260–360 K and Fig. 5 shows the results for five of these temperatures. NQR studies [3,8] have shown that there are three temperature dependent ν_- ^{14}N NQR transitions in this region; at room temperature (298 K) these are at 3359, 3410 and 3458 kHz. As can be seen in Fig. 5 these three transitions are not resolved in the quadrupole dip but two features can be distinguished, for example near 3380 and 3445 kHz for the 301 K data. The resolution of these low and high frequency features decreases at low temperature and they eventually merge. The Arrhenius plot of Fig. 6 shows the temperature dependence of the ^{1}H NMR T_1 values at the minima of the low and high frequency features of the ν_- dip and again there is a step in the plot around 315–320 K. Above this temperature separate linear fits are shown for each resolved feature, they have the same slope from which we obtain E_a as 23 kJ mol^{-1}. For the lower temperature range, a single linear fit is shown and here E_a is 67 kJ mol^{-1}. Below 311 K, the ^{14}N NQR T_1 (T_{1Q}) correlates well with T_1 (^{1}H) at the dip minimum, with $T_{1Q} = 0.1T_1$; above, the coefficient increases by a factor of almost three. The temperature variation of T_1 is similar to that shown in Fig. 3 for the 390 and 510 kHz lines with a marked change in slope near 320 K; above this temperature at a fixed on-dip frequency of 3440 kHz, T_1 shows a linear variation with temperature, with a temperature coefficient of −0.25 ms K^{-1}, close to that for the 510 kHz dip.

A ^{1}H T_1 dispersion measurement across the full range of the ring nitrogen ν_+ transitions is presented in Fig. 7 for RDX at room temperature (298 K). Despite the line broadening, quadrupole dips corresponding to all three ν_+ transitions are resolved at 5110, 5255 and 5300 kHz. At zero-field the three ν_+ ^{14}N NQR lines of RDX at 298 K occur at 5047, 5192 and 5240 kHz [3,8] so the quadrupole dips are Zeeman shifted by about 60 kHz. The minimum in the T_1 dips at level crossing is remarkably deep with values close to 100 ms compared to 100 s off-resonance, a reduction by a factor of 1000, due in large part to the large reduction in the ^{14}N T_{1Q} caused by hindered rotation of the NO_2 groups. We carried out variable temperature measurements in the range 260 to 310 K for the fully resolved dip at 5110 kHz and some of these are also shown in Fig. 7. An Arrhenius plot of the minimum T_1 values at the dips is similar to the lower temperature region of Fig. 6 for the ν_- dip and here a linear fit gives the value of E_a as 72 kJ mol^{-1} close to the ν_- value of 67 kJ mol^{-1}.

3.2. ^{14}N NQR measurements

Fig. 8 is an Arrhenius plot of the temperature variation of the ^{14}N NQR spin–lattice relaxation times T_{1Q} for the three ν_+ and three ν_- transitions of the RDX ring nitrogen atoms in the range 230 to 340 K; the data point symbols are labelled with the room temperature NQR line frequencies. All the T_{1Q} values fall close to the same

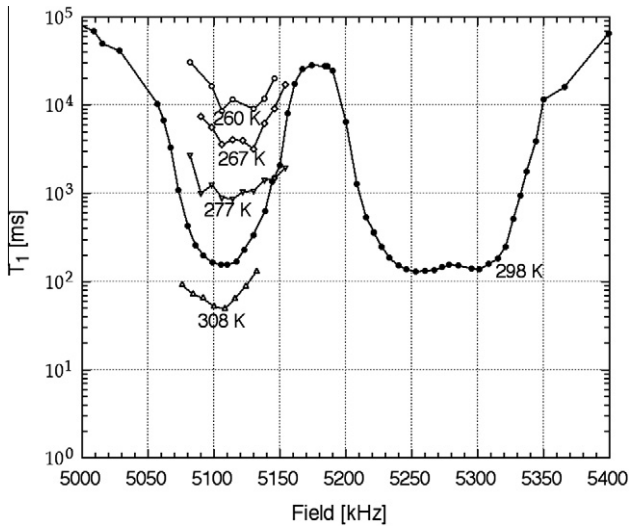

Fig. 7. ^{1}H NMR T_1 dispersion measurement for RDX in the region of the ring nitrogen ν_+ quadrupole dips. Variable temperature results are shown for the low frequency dip.

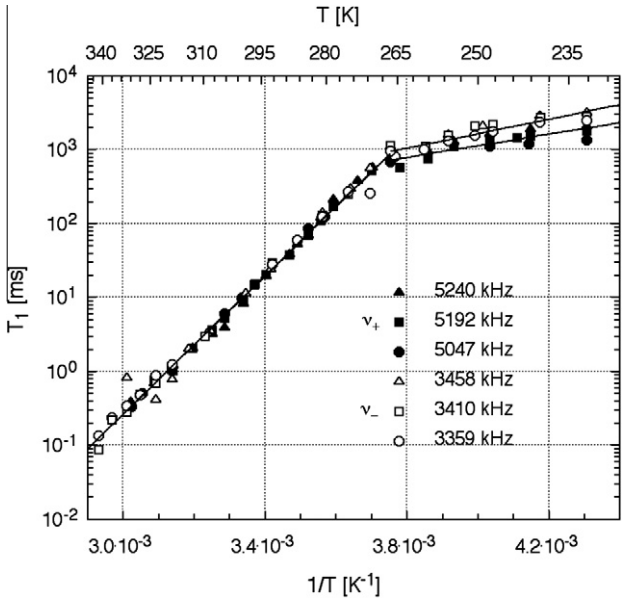

Fig. 8. Arrhenius plot of the temperature variation of the T_{1Q} relaxation time for all six ν_+ and ν_- ^{14}N NQR transitions of the RDX ring nitrogens.

plot, despite the fact that in solid RDX, the plane of the ring C–N–C atoms make different angles, δ, to the corresponding N–N bond, being close to 34° for two of these groups and −20° for the third. It has been argued [3] that the latter should be assigned to N1 in the neutron crystal structure analysis [2] and the former to N2 and N3; further evidence supporting this assignment will be given later. The variation in Fig. 8 falls into two regions with a step near 270 K and from the linear fits using Eq. (6) we obtain an activation energy E_a equal to 90 kJ mol^{-1} above 270 K. Below 270 K there appears to be a slight divergence in the plots for ν_+ and ν_- transitions although the activation energies agree within the experimental error; E_a for the ν_+ group is about 15 kJ mol^{-1} while it is about 19 kJ mol^{-1} for the ν_- group, giving a mean of 17 kJ mol^{-1}.

In the high activation energy region above 270 K these results are consistent with quadrupole relaxation caused by a transient change of the quadrupole parameters of the ring nitrogen nucleus produced by hindered rotation of the attached NO_2 group. The activation energies for this process are very similar for all six transitions despite the different values that the N–NO_2 bonds make with the C–N–C plane. At ambient temperature the ^{14}N NQR spin–lattice relaxation times for the two ν_+ lines of the NO_2 groups are very similar to those of the ring nitrogens, for example at 294 K we have measured T_{1Q} to be 20 ± 3 ms for the lines near 501 and 503 kHz. In PETN T_{1Q} for the NO_2 group ν_+ line is over 1000 times longer and has the lower activation energy of 24.5 kJ mol^{-1}. This difference is ascribed to the larger transient change in the quadrupole parameters for N–NO_2 groups relative to O–NO_2 groups, due possibly to a greater degree of π bonding in the N–NO_2 bond. High activation energies have been observed in a number of aromatic nitro compounds [21], in which the asymmetry parameter of the $^{14}NO_2$ is strongly dependent on the twist angle of its plane with respect to that of the benzene ring [22], with η varying between 0 and 0.4 for twist angles between 90° and 0°. In such cases it is clear that hindered rotation of this group about the C–N bond would produce a significant transient change in the quadrupole parameters. This conclusion is supported by the shortness of the N–N bond in RDX (values of 135 (N1), 139 (N2) and 140 (N3) pm [2]) compared with typical single-bond values, e.g. 145 pm in gaseous hydrazine.

A tentative explanation for the change below 270 K to a region of lower activation energy is that another relaxation mechanism becomes temporally significant. No similar behaviour is observed either in the temperature variation of the NQR frequencies nor other relaxation times; a possible origin might be the onset of an additional contribution to T_{1Q} from magnetic dipole relaxation caused by changes in the ^{14}N···^{1}H dipole–dipole interaction during the hindered rotation of the NO_2 group; it is assumed to pass through an un-resolved broad minimum (or set of minima) between 270 and 230 K. In this case, we estimate from Eq. (1) a mean value τ_c of 0.04 μs, compared to a value of 0.18 μs for the same quantity in PETN at 284 K [14], where the dipolar minimum is well resolved.

The temperature variation of the ^{14}N NQR spin–spin relaxation times T_2 for the three ν_+ and three ν_- transitions of the RDX ring nitrogen atoms is presented in the Arrhenius plot of Fig. 9. Again there are two distinct regions with a step, here to slightly higher temperature near 280 K; above this temperature the linear fit shown in Fig. 9 gives an activation energy of 80 kJ mol^{-1} close, given the experimental scatter, to the 90 kJ mol^{-1} obtained from the T_{1Q} plots. Above about 290 K we see that $T_2 \approx T_{1Q}$ whereas to lower temperature $T_2 < T_{1Q}$ with T_2 tending to an almost constant value of about 0.15 s below 270 K. The T_2 relaxation times were measured from the decay of Hahn echo intensity with increasing RF pulse spacing. In detection applications of NQR multiple pulse sequences are often used to increase signal intensity by the summation of rapidly refocused signals. These sequences are generally either of the steady state free precession (SSFP) type [23], where a constant signal level can be recalled indefinitely, or of the phase-alternated CPMG and pulse spin-locking (PSL) [4,5] type where a train of echo signals can be refocused for as long as the decay time allows. In this latter case the train of echoes decays with an effective relaxation time $T_{2e} > T_2$ which generally increases as the RF pulse spacing decreases. T_{2e} is not a fundamental relaxation time but is a combination of T_2 and T_{1Q} since the echoes are a mixture of Hahn (or direct) and stimulated echoes which introduce the T_{1Q} contribution to T_{2e}. In Fig. 10 the temperature variation of T_{2e} for the ν_+ and ν_- transitions of the RDX ring nitrogen atoms is compared with that of T_{1Q} and T_2, (T_{2e} was measured with a 2 ms refocusing pulse spacing). To low temperature $T_{1Q} > T_{2e} > T_2$ and from near 260 to 305 K

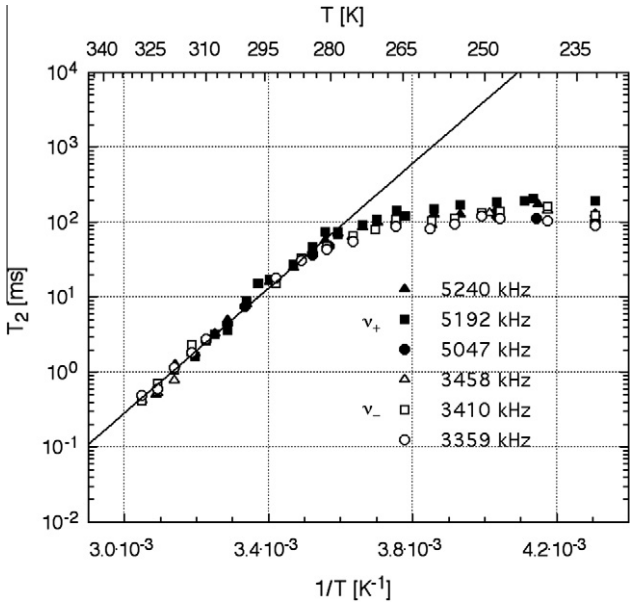

Fig. 9. Arrhenius plot of the temperature variation of the T_2 relaxation time for all six ν_+ and ν_- ^{14}N NQR transitions of the RDX ring nitrogens.

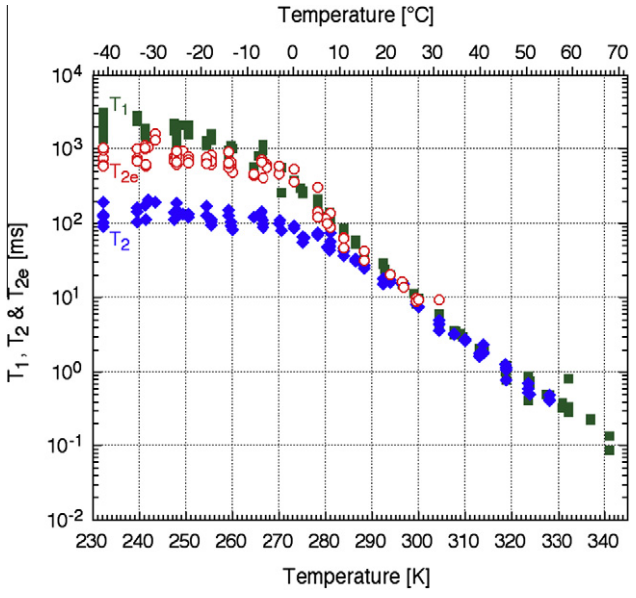

Fig. 10. Comparison of the temperature variation of T_{1Q}, T_2 and T_{2e} for all six ν_+ and ν_- ^{14}N NQR transitions of the RDX ring nitrogens. A colour plot is available in the web version of this article.

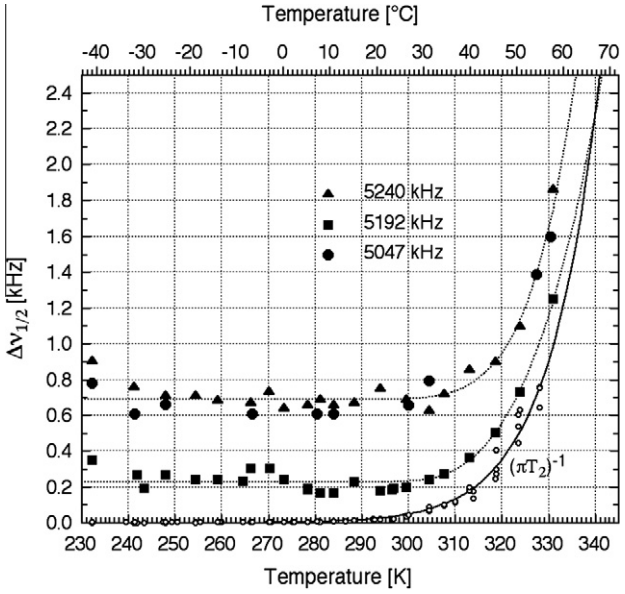

Fig. 11. The temperature variation of the $\Delta\nu_{1/2}$ (FWHH) for the three ν_+ ^{14}N NQR transitions of the RDX ring nitrogens. The natural line width $\Delta\nu_{1/2} = 1/(\pi T_2)$ obtained from the data of Fig. 9 is also plotted –○–. The lines are smoothed interpolations.

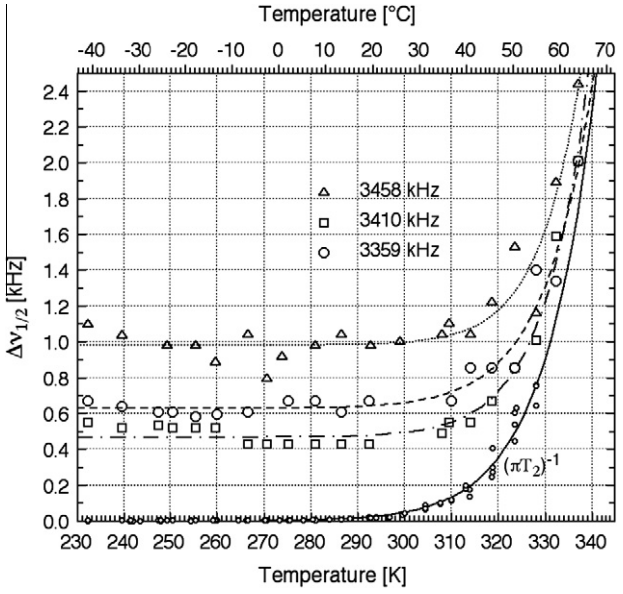

Fig. 12. The temperature variation of the $\Delta\nu_{1/2}$ (FWHH) for the three ν_- ^{14}N NQR transitions of the RDX ring nitrogens. The natural line width $\Delta\nu_{1/2} = 1/(\pi T_2)$ obtained from the data of Fig. 9 is also plotted –○–. The lines are smoothed interpolations.

$T_{2e} = T_{1Q}$ within experimental error. We only have T_{2e} values up to 305 K but all three relaxation times appear to become equal and show the same temperature variation from about 290 K upwards, implying that all three are governed by the same activation energy of around 90 kJ mol^{-1} in this temperature range. The plot also shows that as the temperature gets lower where T_{1Q} is long and $T_{2e} > T_2$ the use of multiple pulse echo sequences for signal enhancement becomes advantageous but to higher temperature where T_{1Q} is short and $T_2 = T_{1Q}$ then steady state free precession (SSFP) sequences are more appropriate.

We have also studied the line widths of the ^{14}N NQR lines of the RDX ring nitrogen atoms. In general NQR line widths are dominated by inhomogeneous broadening and hence vary with the nature of the sample depending on factors such as purity and crystallite size. A careful study of the line shape of the 5192 kHz ν_+ line of RDX in PE4 at room temperature shows that it can be fitted to a Lorentzian function with a full width at half height $\Delta\nu_{1/2}$ of 181.3 Hz. A separate measurement of the signal exponential decay time extracted from the FID signal using the Matrix Pencil technique [24] shows that $T_2^* = 1.755$ ms which gives the same value for the Lorentzian line width using $\Delta\nu_{1/2} = 1/(\pi T_2^*)$. The temperature variation of $\Delta\nu_{1/2}$ for the three ν_+ and three ν_- ^{14}N NQR lines of the RDX ring nitrogen atoms is shown in Figs. 11 and 12 in comparison to a plot of the natural width calculated as $1/(\pi T_2)$ using the data of Fig. 9; smoothed power law interpolations to the data points are also plotted. Within the experimental scatter all the observed line widths show little dependence on temperature from 230 up to about 305 K. Since the observed line shape function is a convolution of the inhomogeneous broadening function, governed by T_2^*, and the natural broadening function, governed by T_2 [25], we assume that in this temperature range the line width is dominated by the former, the natural line width being very narrow. However above 305 K the observed line width begins to broaden before dramatically increasing above 320 K as the natural line width becomes dominant due to the rapid decrease in T_2. The relative temperature variation of T_2^* and T_2 for the ring nitrogen ν_+ lines is compared in Fig. 13, where T_2^* was calculated from the $\Delta\nu_{1/2}$ data of Fig. 11 using $T_2^* = 1/(\pi\Delta\nu_{1/2})$. We assume both contributions to the observed line shape are Lorentzian and write

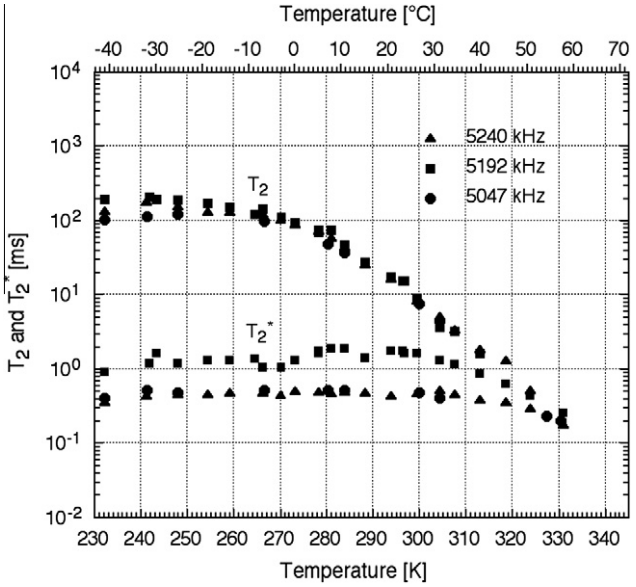

Fig. 13. Comparison of the temperature variation of T_2^*, and T_2 for the three ν_+ ^{14}N NQR transitions of the RDX ring nitrogens.

$$1/T_2^* = 1/T_{2(Inhom)} + 1/T_2 \tag{7}$$

Figs. 14 and 15 show the temperature dependence of $1/T_{2(Inhom)}$ below 320 K for the three ν_+ and ν_- lines of the RDX ring nitrogen atoms calculated from our measured T_2 and T_2^* (from $\Delta\nu_{1/2}$) values using Eq. (7). At low temperature T_2 is long so we can write $(1/T_{2(Inhom)})_{T=0} = (1/T_2^*)_{T=0}$ and this applies until T_2 has decreased to a point where it approaches $(T_2^*)_{T=0}$ and begins to reduce T_2^*. Over the temperature range of Figs. 14 and 15 we assume T_2 has little influence so the linear fits shown represent the temperature dependence of $1/T_{2(Inhom)}$ written as

$$1/T_{2(Inhom)}(T) = \left(1/T_2^*\right)_{T=0} + \alpha T \tag{8}$$

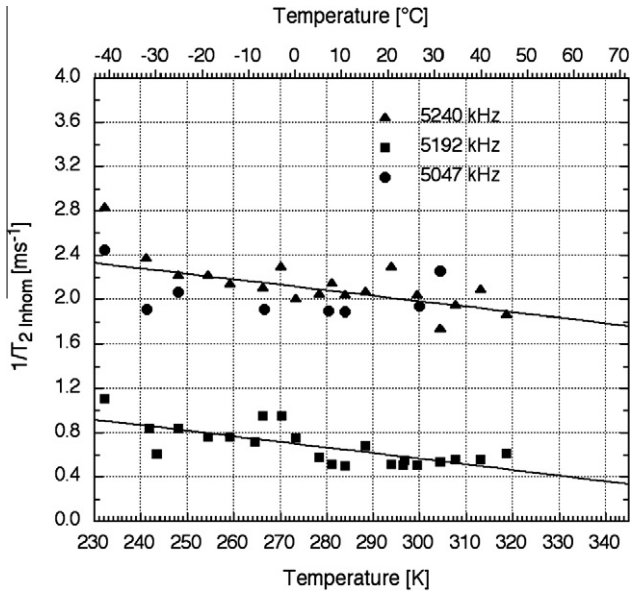

Fig. 14. The temperature dependence of $1/T_{2(Inhom)}$ for the three ν_+ lines of the RDX ring nitrogens calculated from our measured T_2 and T_2^* (from $\Delta\nu_{1/2}$) values.

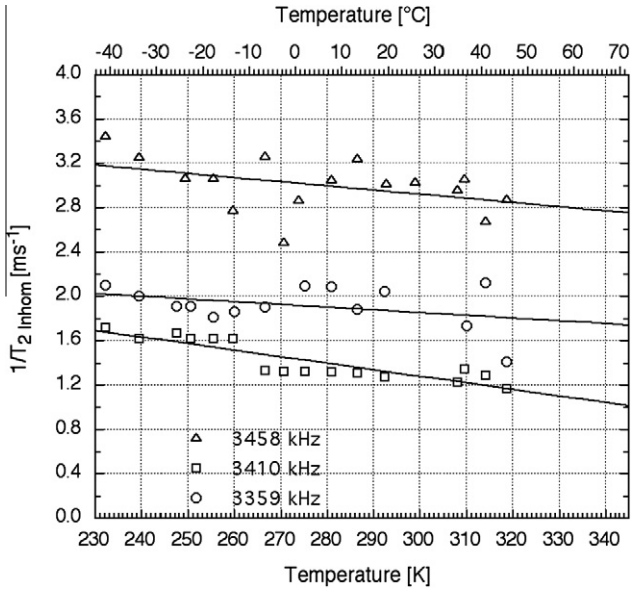

Fig. 15. The temperature dependence of $1/T_{2(Inhom)}$ for the three ν_- lines of the RDX ring nitrogens calculated from our measured T_2 and T_2^* (from $\Delta\nu_{1/2}$) values.

The temperature coefficients α of $1/T_{2(Inhom)}$ are -0.0051 and $-0.0049\ ms^{-1}K^{-1}$ for the 5192 kHz line and the 5240/5047 kHz lines (fitted together) and -0.0037, -0.0059 and $-0.0025\ ms^{-1}K^{-1}$ for the 3458, 3410 and 3359 kHz lines respectively.

Three-frequency secondary echo NQR experiments [26] on the 5047 kHz line of RDX (tentatively assigned to the N2 atom in the crystal structure analysis) in the propellant XM39 (75% RDX) have shown that the frequency broadening functions $\Delta\omega(V_{zz})$ and $\Delta\omega(V_{xx}–V_{yy})$, where V_{zz} is the maximum principal component of the electric field gradient and V_{xx} and V_{yy} the other two components, consist of two terms, one correlated and the other uncorrelated, the former having a correlation coefficient of -10% at 300 K. The negative sign of this coefficient could be understood if a significant contribution to $\Delta\omega$ comes from the $2p_\pi$ electrons on the ring nitrogen atom. V_{zz} is then likely to lie close to parallelism with the direction of the lone pair, with the other two components V_{xx} and V_{yy} lying in the perpendicular plane, where

$$V_{zz} = np\begin{pmatrix} -1/2 & 0 & 0 \\ 0 & -1/2 & 0 \\ 0 & 0 & 1 \end{pmatrix} \tag{9}$$

in which n is the occupation number of the $2p_\pi$ orbital and p is the electric field gradient generated by a single $2p_\pi$ electron. Any variation in V_{zz} then has a negative correlation with that of V_{xx} and V_{yy}. The finite but small value of $\Delta\omega(V_{xx}–V_{yy})$ is presumably due to the lack of axial symmetry about the direction of V_{zz}.

The most likely origin of the temperature dependence of $1/T_{2(Inhom)}$ as in Eq. (8) is the change in the $2p_\pi$ electron distribution at the ring nitrogen caused by the torsional motion of the attached NO_2 group which changes the degree of π-bonding. High pressure ^{35}Cl NQR studies of 1,3,5-trichlorobenzene [27] have demonstrated the sensitivity of the $3p_\pi$ lone pair electron distribution on the chlorine atom to changes in torsional frequencies and electron polarisation effects at high pressure. So it is reasonable to assume that environmental effects at defects could also produce similar changes in the $2p_\pi$ distribution at the ring nitrogen atom which would vary with temperature.

The temperature dependence of NQR line frequencies is known to be governed by the averaging effects of molecular vibrations and librations on the electric field gradient [28].The frequencies themselves could be detected by terahertz [11] and Fourier transform or photoacoustic infra-red spectroscopy [10], but as yet no agreed assignments to N–NO_2 torsional modes have been made; they have been predicted to lie at 62 and 102 kHz which may correspond to signals at 66 and 103 cm^{-1} in the terahertz spectrum [11]. In RDX, we assume that the maximum principal component q_{zz} of the electric field gradient of the ring ^{14}N lies close to the direction of the $2p_\pi$ orbital with the smallest value q_{xx} parallel to the N–N bond For simple harmonic motion the temperature variations of the two NQR frequencies ν_+ and ν_- are given [29] by the equations

$$\begin{aligned}(d\omega_+/dT) &= e^2qQ/4\hbar[-2(3+\eta)d\langle\theta_x^2\rangle_{Av}/dT - (3-\eta)d\langle\theta_y^2\rangle_{Av}/dT \\ &\quad - 2\eta d\langle\theta_z^2\rangle_{Av}/dT] \\ (d\omega_-/dT) &= e^2qQ/4\hbar[-(3+\eta)d\langle\theta_x^2\rangle_{Av}/dT - 2(3-\eta)d\langle\theta_y^2\rangle_{Av}/dT \\ &\quad + 2\eta d\langle\theta_z^2\rangle_{Av}/dT]\end{aligned} \tag{10}$$

where $\langle\theta_x^2\rangle_{Av}$, $\langle\theta_y^2\rangle_{Av}$ and $\langle\theta_z^2\rangle)_{Av}$ are the mean square torsional angles about the principal x, y, z axes. We assume that the same equations will apply when ω is replaced by $\Delta\omega$ and the three mean torsional amplitudes are replaced by the respective mean square distributions in the torsional angles $\langle\theta_x^2\rangle_{Av}$, $\langle\theta_y^2\rangle_{Av}$ and $\langle\theta_z^2\rangle_{Av}$ at crystal defects or impurities, since the two sets represent independent and random processes. For small angles, these equations were evaluated assuming a mean value of 5700 kHz for (e^2qQ/h) and 0.61 for η and neglecting the first term on the right hand side for torsional motion about q_{xx} The results are shown in Table 1. With this model, N1 has the widest difference between the temperature coefficients of the torsional angle distributions and a large difference between the two ratios, suggesting that N1 is much more affected at crystal defects than N2 and N3. The ratios in the last column should provide an approximate estimate of the ratio of the squares of the torsional frequency to its frequency distribution. Assuming [29] that

$$d\langle\theta^2\rangle_{Av}/dT = k/4\pi^2\nu_t^2 I_t \tag{11}$$

and that the torsional frequency observed at of 62 cm^{-1} belongs to N2 and N3, because of the longer N–N bond length, we estimate approximate values for the torsional frequency distributions near defects of 4.9 cm^{-1} for N2 and 5.2 cm^{-1} for N3. Theoretical calculations on solid RDX suggest that the most likely defects are either a molecular vacancy [30] or an edge dislocation [31]. The latter,

Table 1
Temperature dependence of the mean square angles and distributions for the three ^{14}N lines assuming q_{xx} lies along the N–N bond, units are 10^{-6} K^{-1}. The last two columns give the ratios of the temperature coefficients of the mean square torsional angles, θ_y and θ_z, to their distributions.

	$d\langle\theta_y^2\rangle_{Av}/dT$	$d\langle\Delta\theta_y^2\rangle_{Av}/dT$	$d\langle\theta_z^2\rangle_{Av}/dT$	$d\langle\Delta\theta_z^2\rangle_{Av}/dT$	Ratio (θ_y)	Ratio (θ_z)
N1	12.7	0.0854	38.3	0.0646	149	593
N2	19.6	0.0576	30.7	0.1130	339	272
N3	20.1	0.0676	32.6	0.0934	297	349

together with impurities such as occluded solvent, are consistent with the similarity of the effects at N2 and N3 and the rather different behaviour observed for N1, due to its higher effective negative atomic charge relative to N2 and N3 [32] and the two rather short intermolecular O···H distances of 246 and 248 pm of the attached NO_2 oxygen atoms to the hydrogen atoms of neighbouring CH_2 groups [2]. These intermolecular bonds might well be broken at edge dislocations and close to impurities.

For rigid ring atoms, as assumed in the neutron crystal structure analysis [2], the values of $d\langle\theta_z^2\rangle/dT$ and $d\langle\theta_y^2\rangle$ should be very similar for all three atoms, but their values in Table 1 all differ significantly, suggesting that a significant change in the ring geometry accompanies the torsional motion about the N–NO_2 bond, the most likely of which is a change in the interplanar angle δ, which is known to vary from one phase to the next [1] and even on application of high pressure [33]. Approximate values of the temperature coefficients of its mean square values can be obtained by subtracting the corresponding quantities in Table 1, giving values for $d\langle\delta^2\rangle/dT$ of 25.7 for N1, 11.1 for N2 and 12.5 for N3, all in units of 10^{-6} K^{-1}. The corresponding changes in the distributions $d\langle\Delta\delta^2\rangle/dT$ are −0.0208 for N1, +0.0556 for N2 and +0.0258 for N3 in the same units; in this case, the ratios of the two quantities are N1 − 1234, N2 + 200 and N3 + 498, corresponding to the different values measured for δ in the neutron crystal structure analysis [2]. Again the unusual values of these quantities for N1 distinguish it sharply from the other two nitrogen atoms, possibly due to the short intermolecular contacts of the attached NO_2 to hydrogen atoms on neighbouring CH_2 groups.

There is evidence in the literature [34] that RDX samples of different origins have significantly different line widths, suggesting that the kind of analysis summarised above might provide useful information on the stability of a sample with respect its stability in storage and for seized samples, even its likely origin.

4. Conclusions

We have shown that most, if not all, of the temperature dependencies of the ^{14}N NQR frequencies, relaxation times and line widths of the $^{14}NO_2$ groups in the RDX molecule in the solid phase are governed by hindered rotation of the NO_2 groups about the N–NO_2 bond with an activation energy close to 92 kJ mol^{-1}, together with their torsional frequencies about the same bond. The temperature dependence of the line widths of the three 3.4 and 5.2 MHz lines between 230 and 320 K can be explained by changes in the frequency distribution of the torsional oscillation amplitudes of the NO_2 group about the N–NO_2 bond at crystal defects, their relative values being consistent with the latter being due mainly to edge dislocations or impurities in the samples studied. The ^{1}H T_1 dispersion shows deep quadrupole dips at both the nitro and ring nitrogen NQR frequencies; above 310 K, the T_1 values at these dips are governed by the spin mixing time between the ^{1}H Zeeman and the ^{1}H/^{14}N spin–spin levels.

Acknowledgments

We thank the Defence Science and Technology Laboratory at Fort Halstead, UK for support of this project and Dr. Erik Gudmunson for his advice and comments. We are also grateful to an unknown referee for suggesting changes to a few of the figures which has improved their clarity.

References

[1] A.J. Davidson, I.D.H. Oswald, D.J. Francis, A.R. Lennie, W.G. Marshall, D.I.A. Millar, C.R. Pulham, J.E. Warren, A.S. Cumming, Explosives under pressure—the crystal structure of γ-RDX as determined by high-pressure X-ray and neutron diffraction, CrystEngComm. 10 (2008) 162–165.
[2] C.S. Choi, E. Prince, The crystal structure of cyclotrimethylene – trinitramine, Acta Cryst. B 28 (1972) 2857–2862.
[3] R.J. Karpowicz, T.B. Brill, Librational motion of hexa-hydro-1,3,5-trinitro-s-triazine based on the temperature dependence of the nitrogen-14 nuclear quadrupole resonance spectra : the relationship to condensed-phase thermal decomposition, J. Phys. Chem. 87 (1983) 2109–2112.
[4] S.M. Klainer, T.B. Hirschfeld, R.A. Marino, Fourier Transform Nuclear Quadrupole Resonance Spectroscopy, in: Fourier, Hadamard and Hilbert Transforms in Chemistry, Plenum Press, New York, 1982.
[5] R.A. Marino, S.M. Klainer, Multiple spin echoes in pure quadrupole resonance, J. Chem. Phys. 67 (1977) 3388–3389.
[6] D.F. Lee, H. Itozaki, M. Tachiki, Improving the sensitivity of a high-T_c SQUID at MHz frequency using a normal flux transformer, Supercond. Sci. Technol. 19 (2006) S231–S234.
[7] V.S. Grechishkin, New methods of nuclear quadrupole resonance, Z. Naturforsch. 45a (1990) 559–564.
[8] J.A.S. Smith, M.D. Rowe, R.M. Deas, M.J. Gaskell, Nuclear quadrupole resonance detection of landmines, in: The Proceedings of EUDEM2-SCOT-2003, International Conference on Requirements and Technologies for the Detection, Removal and Neutralization of Landmines and UXO VUB, Brussels, Belgium, vol. 2, 2003, pp. 715–721.
[9] A.G. Landers, T.M. Apple, C. Dybowski, T.B. Brill, ^{1}H nuclear magnetic resonance of α-hexahydro-1,3,5-trinitro-s-triazine (RDX) and the α-, β-, γ- and δ-polymorphs of octahydro-1,3,5,7-tetranitro-1,3,5,7-tetrazocine (HMX), Magn. Reson. Chem. 23 (1985) 158–160.
[10] F. Huang, B. Schulkin, H. Altan, J.F. Federici, D. Gary, R. Barat, D. Zimdars, M. Chen, D.B. Tanner, Terahertz study of 1,3,5-trinitro-s-triazine by time-domain and Fourier transform infrared spectroscopy, Appl. Phys. Lett. 85 (2004) 5535–5537.
[11] D.G. Allis, J.A. Zeitler, P.E. Tady, T.M. Korter, Theoretical analysis of the terahertz solid-state spectrum of the high-explosive RDX, Chem. Phys. Chem. 7 (2006) 2398–2408.
[12] M.R. Leahy-Hoppa, M.J. Fitch, X. Zheng, L.M. Hayden, R. Osiander, Wideband terahertz spectroscopy of explosives, Chem. Phys. Lett. 434 (2007) 227–230.
[13] R.L. Prasad, R. Prasad, G.C. Bhar, S.N. Thakur, Photoacoustic spectra and modes of vibration of TNT and RDX at CO_2 laser wavelengths, Spectrochim. Acta 58A (2002) 3093–3102.
[14] J.A.S. Smith, T.J. Rayner, M.D. Rowe, J. Barras, N.F. Peirson, A.D. Stevens, K. Althoefer, Magnetic field-cycling NMR and ^{14}N, ^{17}O quadrupole resonance in the explosive pentaerythritol tetranitrate (PETN), J. Magn. Reson. 204 (2010) 139–144.
[15] W.L. Rollwitz, J.D. King, S.D. Shaw, Determining the Potential of Radiofrequency Resonance Absorption Detection of Explosives Hidden in Airline Baggage, FAA Report FA-RD-76-29, Washington, DC, 1975.
[16] W.L. Rollwitz, J.D. King, G.A. Matzkanin, Fundamentals of Nuclear Magnetic Resonance for the Detection and Identification of Explosives, in: Proc. New Concepts Symposium. Workshop on the Detection and Identification of Explosives, Quantico, Va, USA, 1978.
[17] M.L. Buess, A.N. Garroway, Nuclear Quadrupole Resonance (NQR) Method and Apparatus for Detecting a Nitramine Explosive, US Patent 6104109, August 15, 2000.
[18] K.R. Thurber, K.L. Sauer, M.L. Buess, C.A. Klug, J.B. Miller, Increasing ^{14}N NQR signal by ^{1}H–^{14}N level crossing with small magnetic fields, J. Magn. Reson. 177 (2005) 118–128.
[19] G.W. Leppelmeier, E.L. Hahn, Nuclear dipole field quenching of integer spins, Phys. Rev. 141 (1966) 724–731.
[20] D. Stephenson, J.A.S. Smith, Nitrogen-14 quadrupole cross-relaxation spectroscopy, Proc. R. Soc. London, A 416 (1988) 149–178.
[21] J. Schneider, C.A. Meriles, I.A.de O. Nunes, S.C. Perez, The dynamics of the NO_2 group in the solid phase of m-chloronitrobenzene studied by Raman Spectroscopy and ^{35}Cl NQR, J. Mol. Struct. 447 (1998) 13–19.
[22] A. Weiss, The combination of X-ray diffraction and nuclear quadrupole resonance studies of crystals, Acta. Cryst. B 51 (1995) 523–539.

[23] M.L. Buess, A.N. Garroway, J.P. Yesinowski, Removing the Effects of Acoustic Ringing and Reducing Temperature Effects in the Detection of Explosives by NQR, US Patent 5365171, November 15, 1994.
[24] Y.-Y. Lin, P. Hodgkinson, M. Ernst, A. Pines, A novel detection–estimation scheme for noisy NMR signals: applications to delayed acquisition data, J. Magn. Reson. 128 (1997) 30–41.
[25] J. Dolinšek, F. Milia, G. Papavassiliou, G. Papantopoulos, M. Karayianni, Two dimensional NQR separation og inhomogeneous and homogeneous lineshapes in disordered solids, Appl. Magn. Reson. 6 (1994) 499–510.
[26] K.L. Sauer, B.H. Suits, A.N. Garroway, J.B. Miller, Secondary echoes in three-frequency nuclear quadrupole resonance of spin-1 nuclei, J. Chem. Phys. 118 (2003) 5071–5081.
[27] L.V. Jones, M. Sabir, J.A.S. Smith, ^{35}Cl quadrupole resonance in 1,3,5-trichlorobenzene at high pressure, J. Chem. Soc. Farad. Trans. 2 74 (1978) 1723–1734.
[28] H. Chihara, N. Nakamura, Study of molecular motion by nuclear quadrupole resonance and relaxation, Adv. Nucl. Quad. Reson. Ed. J.A.S. Smith 4 (1980) 1–69.
[29] B.L. Barton, Influence of torsional motions on the quadrupole resonance lines of ^{14}N in piperazine, J. Chem. Phys. 46 (1967) 1553–1556.
[30] M.M. Kuklja, A.H. Kuntz, Ab Initio simulation of defects. Part 1. Molecular vacancy structure in RDX crystal, J. Phys. Chem. Solids 61 (2000) 35–44.
[31] M.M. Kuklja, Electronic structure modifications induced by nanosize lattice imperfections in molecular crystals, Comp. Nanosci. (2001). ISBN 0-9708275-3-9.
[32] R. Pati, S. Srinivas, T. Briere, T.P. Das, N. Sahoo, S.N. Ray, First principles investigation of nitrogen nuclear quadrupole interactions in the RDX ($C_3H_6N_6O_6$) system, J. Phys. Chem. 99 (1995) 9051–9055.
[33] S.M. Peiria, R. Butcher, W. Pearson, X-ray Diffraction Study of Single Crystals at High Pressure Using Synchrotron Radiation, Joint AIRAPT/EHPRG Meeting, Karlsruhe, 2005.
[34] M.L. Buess, S.M. Calder, Factors affecting the NQR line widths in nitramine explosives, Appl. Magn. Reson. 25 (2004) 383–393.